Dalton Transactions

Investigation of Vanadium(III) and Vanadium(IV) Compounds Supported by the Linear Diaminebis(phenolate) Ligands. Correlation Between Structures and Magnetic Properties.

Journal:	*Dalton Transactions*
Manuscript ID	DT-ART-12-2020-004302.R2
Article Type:	Paper
Date Submitted by the Author:	03-Mar-2021
Complete List of Authors:	Janas, Zofia; University of Wrocław, Faculty of Chemistry Jezierska, Julia; University of Wroclaw, Faculty of Chemistry Ozarowski, Andrew; Florida State University, National High Magnetic Field Laboratory Bieńko, Alina; University of Wroclaw, Faculty of Chemistry Lis, Tadeusz; Wrocław University, F. Joliot-Curie 14, Faculty of Chemistry Jezierski, Adam; University of Wrocław, Faculty of Chemistry Krawczyk, Marta; Wrocław Medical University, Department of Analytical Chemistry, Faculty of Pharmacy

ARTICLE

Investigation of Vanadium(III) and Vanadium(IV) Compounds Supported by the Linear Diaminebis(phenolate) Ligands. Correlation Between Structures and Magnetic Properties.

Received 00th January 20xx,
Accepted 00th January 20xx

DOI: 10.1039/x0xx00000x

Zofia Janas,[a] Julia Jezierska,[a] Andrew Ozarowski,*[b] Alina Bieńko, *[a] Tadeusz Lis,[a] Adam Jezierski[a] and Marta Krawczyk[c]

A family of oxidovanadium(IV) compounds carrying the linear diaminebis(phenolate (salans) $L^{1–5}$ ligands {L^1 = $[MeNCH_2CH_2NMe(CH_2–4–CMe_2CH_2CMe_3–C_6H_3O)_2]^{2–}$; L^2 = $[MeNCH_2CH_2NMe(CH_2–4–CH_3–C_6H_3O)_2]^{2–}$; L^3 = $[MeNCH_2CH_2NMe$-$(CH_2–4–Cl–C_6H_3O)_2]^{2–}$; L^4 = $\{MeNCH_2CH_2NMe[CH_2–4,6–(CH_3)_2–C_6H_2O]_2\}^{2–}$; L^5 = $\{MeNCH_2CH_2NMe[CH_2–4,6–(Br)_2–C_6H_2O]_2\}^{2–}$ and non–oxidovanadium(III) with $L^{2,4}$ and acac ligands has been prepared and characterized by chemical and physical techniques. Reactions of $[VO(acac)_2]$ with ligand precursors $H_2L^{2,4}$ in toluene or hexane afforded vanadium(III) compounds [V(L–κ⁴ONNO)(acac)] (**1**, L^2; **2**, L^4), while the use of acetonitryle or ethanol led to the formation of dimeric oxidovanadium(IV) $[(VO)_2(\mu–L–\kappa^4ONNO)_2]$ (**3**, L^1; **4**, L^2; **5**, L^3) and monomeric [VO(L–κ⁴ONNO)] (**6**, L^4, **7,** L^5) compounds. As shown by X–ray crystallography, compounds **1** and **2** are monomeric, in which the chelating ligands afford octahedral *cis*–α geometry at the vanadium center. In the dimeric structures of **3**–**5**, the six–coordinate vanadium centers are bridged via two oxygen atoms of the $L^{1–3}$ ligands while the **$L^{4,5}$** ligands generate square pyramidal structure of the monomeric **6** and **7** compounds. HFEPR studies allowed to determine the spin Hamiltonian parameters of the S=1 spin state of the monomeric V(III) and dimeric V(IV), and S=$^1/_2$ in monomeric V(IV) compounds. Magnetic measurements of **3**–**5** indicated weak ferromagnetic metal-metal exchange interactions. A reaction course for the deoxygenation and reduction of vanadyl–salan compounds is proposed.

The chemistry of vanadium compounds with tetradentate ONNO ligands like Schiff bases (salens) and diaminebis(phenolate) (salans) is of persistent interest to chemists in context of their relevance to bioinorganic chemistry,[1] molecular magnetism,[2] catalysis,[3] and prospective therapeutic applications.[3b,4] Among them, those containing salen ligands have mostly been studied. In the last decade, increasing attention has been paid to the salan ligands, a salen–reduced variants, which have increased flexibility, stronger nitrogen donors and greater resistance to hydrolysis than their salen analogues. These features, together with the stabilizing character of the hard phenolate oxygen allowed to create a significant number of oxidovanadium(V) [VO(L-κ⁴O,N,N,O)(OR)] compounds with general formula [VO(salan)(OR)] (R = alkyl, aryl). In most cases, the N-methylated ligands with different substituents at the ortho and para positions of the aromatic rings generate octahedral either monomeric or dinuclear V(V) compounds adopting cis-α geometry in the solid state, and only one of them has the *cis*-β-type structure.[3d,4b,5] So far, only a few oxidovanadium(IV) and no V(III) salan compounds have been described.[5a,d–f] The polynuclear linear chain structures (···V=O···V=O···) have been postulated for $V^{IV}O$ compounds with different salan type ligands, including those derived from chiral diamines, diaminecyclohexane and diphenylethylenediamine, pursuant to low μ_{eff}, ν(V=O) values and the EPR spectra. [5d–f] Synthetic route to the aforementioned compounds involved the reaction of $VOCl_2$ or $VOSO_4$ with an appropriate H_2salan in a basic medium. Previously, our research group has succeeded in the preparation of a series of the $[V^{IV}O(salan)]$ {salan = L^1= $[MeNCH_2CH_2NMe(CH_2–4–CMe_2CH_2CMe_3–C_6H_3O)_2]^{2–}$; L^2 =$[MeNCH_2CH_2N–Me(CH_2–4–CH_3C_6H_3O)_2]^{2–}$; L^3 = $[MeNCH_2CH_2$.NMe-$(CH_2–4–Cl–C_6H_3O)_2]^{2–}$} compounds by the reduction of $[V^VO(salan)(OR)]$ (R = Me, Et) with *N*-Methyl-*N*-phenylhydrazine (NH_2NMePh).[5a] These previous studies were generally devoted to the potential of salan ligands in the creation of compounds mimicking the active centers of vanadium nitrogenase. Observation of salan-based vanadium(V) compounds oxidizing NH_2NMePh to 2-tetrazene ($N_4Me_2Ph_2$) has been crucial for better understanding of the biological formation of hydrazine. It was then demonstrated very clearly by EPR spectra and magnetic studies that all except one $V^{IV}O$ compounds, which are the products of $[V^VO(salan)(OR)]$ reduction, are formed as insoluble powders containing a mixture of monomeric (S = $^1/_2$) and dimeric (S = 1) species. Their high stretching frequency ν(V=O) at ca. 947 - 960 cm^{-1} excluded the polynuclear (···V=O···V=O···) structures. The monomeric structure was revealed for ~~only one~~ [VO(salan)]·EtOH

[a] *Faculty of Chemistry, University of Wrocław, 14, F. Joliot–Curie, 50–383 Wrocław, Poland, e-mail: alina.bienko@chem.uni.wroc.pl*
[b] *National High Magnetic Field Laboratory, Florida State University, 1800 E. Paul Dirac Drive, Tallahassee, FL 32310 USA, e-mail: ozarowsk@magnet.fsu.edu*
[c] *Faculty of Pharmacy, Wrocław Medical University, 211 Borowska, 50–556 Wrocław, Poland*
Electronic Supplementary Information (ESI) available: [Additional crystallographic data for 1, 2, 3–6; X-band and HF EPR spectra for 3–7 and for 2, respectively; additional magnetic data for 3–5 (PDF), XRD data for 1, 2 and 3–7 (CIF).]. See DOI: 10.1039/x0xx00000x

{salan = L^1=[$MeNCH_2CH_2NMe(CH_2$–4–$CMe_2CH_2CMe_3$–$C_6H_3O)_2]^{2-}$ } by the X–ray study and at that time, it was the only example of structurally characterized [$V^{IV}O$(salan)] compound.[5a]

Therefore, this new work was undertaken to find other synthetic methods of salan – based oxidovanadium(IV) complexes to prepare their crystals in dimeric or monomeric form separately by using various solvents and H_2salans differently substituted in aromatic rings, either para in H_2L^{1-3} or ortho and para in new H_2L^4= {$MeNCH_2$-$CH_2NMe[CH_2$–4,6–$(CH_3)_2$–$C_6H_2OH]_2\}^{2-}$ and H_2L^5 = {$MeNCH_2CHNMe[CH_2$–4,6–$(Br)_2$–$C_6H_2OH]_2\}^{2-}$). The search for selective and efficient synthesis allowed us to discover the decisive influence of solvent polarity on the reaction between $V^{IV}O(acac)_2$ and H_2salan ligands, giving in non-polar solvents the crystals of monomeric V^{III}(salan)(acac) compounds, where salan=L^2, **1** and L^4, **2** and in non -polar solvents the $V^{IV}O$(salan) compounds as dimers with salan = L^1, **3**; L^2, **4** and L^3, **5** and as monomers with salan = L^4, **6** and L^5, **7** as solid. We also developed a number of other alternative synthetic methods which revealed and confirmed the likely causes of the various products of above reaction depending on the solvents and salan substitution. We also present here the results of the HFEPR and magnetic studies of these seven new oxidovanadium(IV) and non-oxidovanadium(III) complexes in correlation with their crystal and molecular structure properties.

Results and Discussion

Synthesis of the non–oxidovanadium(III) and oxido-vanadium(IV)–salan compounds.

To synthesize the oxidovanadium(IV) compounds based on the salan ligands, [$V^{IV}O(acac)_2$] was used as the vanadium precursor and various solvents such as toluene, n-hexane, acetonitrile and ethanol. Unexpectedly, when [$V^{IV}O(acac)_2$] was refluxed with equimolar quantities of $H_2L^{2,4}$ in toluene or n-hexane, orange solids of non–oxidovanadium(III) compounds [$V^{III}(L^{2,4}$–κ^4ONNO)(acac)] (L^2, **1**; , L^4, **2**) were obtained with ~ 50% yield (**method 1** in Scheme 1). The use of [$V^{III}(acac)_3$] instead of [$V^{IV}O(acac)_2$] (**method 2** in Scheme 1) improved yield to 70.0% **1**, 91.5 %; **2** ~~to above 70%.~~ However, refluxing [$V^{IV}O(acac)_2$] with H_2L^{1-5} in acetonitrile or ethanol resulted in the formation of light–violet compounds [$(V^{IV}O)_2(\mu$–L^{1-3}–κ^4ONNO)$_2$] (L^1, **3**; L^2,**4**; L^3, **5**) and [$V^{IV}O(L^{4,5}$–κ^4ONNO)] (L^4, **6**; L^5,**7**) with 50–70% yield (according to *Method A*, see Experimental). When the above reactions were carried out at room temperature, the formation of desired products was not complete and unreacted [$V^{IV}O(acac)_2$] or [$V^{III}(acac)_3$], respectively, was observed in the post–reaction mixture. To confirm the effect of substituents at the ortho position in the salan ligand L on the reduction of vanadium(V) to vanadium(IV) by hydrazine derivatives, compounds **6** and **7** were also prepared *via* the reaction of *in situ* generated [$V^{V}O(L^4$–κ^4ONNO)(OPr)] with NH_2NMe_2 in CH_3CN at room temperature, in a manner similar to that described previously[5a] (according to *Method* B, see Experimental) with yield 85.7%, **6**; 98.0%, **7**. Compounds **1** and **2** are very well soluble in CH_3CN and toluene, and insoluble in *n*-hexane. They are air– and moisture–sensitive both in solution and in the solid state and have to be stored under inert atmosphere. In contrast, compounds **3**–**5** are stable in air for several days but their solubility in organic solvents is very limited. The synthetic method presented here was successful in obtaining crystals of **3**–**7** directly by slow cooling of the post–reaction mixture. It is worth emphasizing that a previously described preparation of compounds **3-5** via the reduction of appropriate vanadate precursors by NH_2NMe_2 in n-hexane resulted in their isolation as completely insoluble powders.[5a] However, as was shown by EPR spectra and magnetic measurements in Ref. 5a and was confirmed in this work, both methods produced **3**–**5** as a mixture of monomeric and dimeric forms (Scheme 1) and only the crystals of dimers were suitable for crystallographic studies. The monomeric form of **5** was previously isolated from ethanolic solution and identified by the X–ray crystallography.[5a]

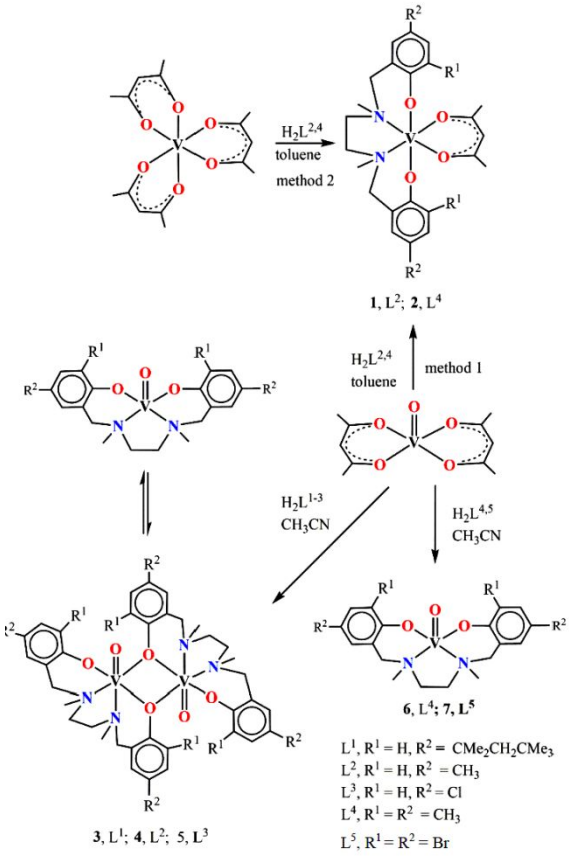

Scheme 1. Synthetic strategy for compounds **1–7**

The results of reactions between [$V^{IV}O(acac)_2$] and H_2L^{1-5} indicate that the kind of solvent strongly ~~affects~~ determines the course of the reaction and its product. In polar solvents such as acetonitrile or ethanol, the substitution of the $(acac)^-$ groups in [$VO(acac)_2$] by the $(L^{1-5})^{2-}$ ligands with elimination of H^+ and $(acac)^-$ occurs to afford vanadyl compounds **3–7** (according to *Method* A, see Experimental). Thus, the question now arises, why the reactions of [$VO(acac)_2$] with $H_2L^{2,4}$ produce non-oxido vanadium(III) compounds **1** and **2** in non-polar solvents, toluene or n-hexane, respectively. To answer

this question, the impact of protons eliminated from $H_2L^{2,4}$ and Hacac during the reaction had to be considered. A probable course of formation of **1** and **2** in toluene or n-hexane is proposed in Scheme 2. Compound **4,** a mixture of dimeric and monomeric forms, is presented in this Scheme as monomer for simplicity. However, the existence of **4** as monomer in solution was confirmed by EPR spectrum (Fig. S12).

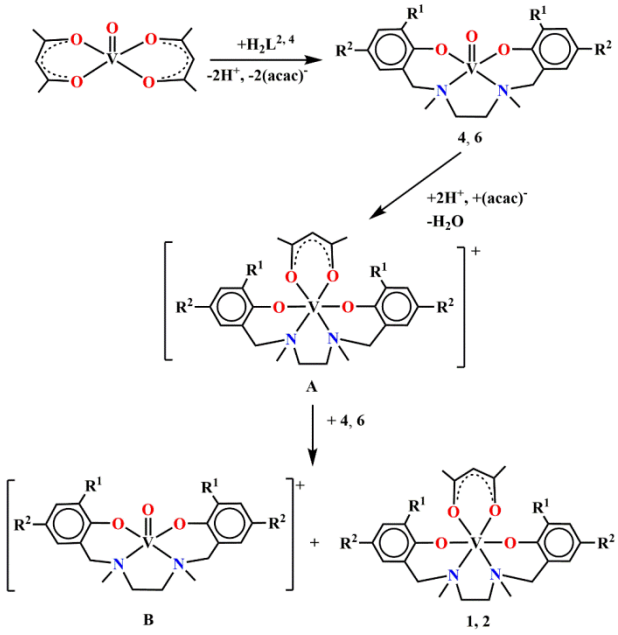

Scheme 2. A plausible reaction course for the formation of **1** and **2** in toluene or *n*–hexane.

It is quite likely that in the first stage of the reaction the oxido-vanadium(IV) compounds **4** or **6** are formed by an alcoholysis of the V–O(acac) bonds by $H_2L^{2,4}$ and elimination of H^+ and $(acac)^-$ ions. Next, the protonation of the oxido ligand in **4** or **6** by H^+ (from $H_2L^{2,4}$ and Hacac as weak acids) followed by deoxygenation and release of H_2O and $(acac)^-$ most likely lead to non–oxidovanadium(IV) cationic species A (Scheme 2). Although the intermediate compounds A have not been isolated, their formation was well documented in vanadium chemistry by the reactivity of the V=O moiety with polydentate phenols, including their derivatives functionalized with X-donor atom (X = N, S, Se, P).[6,7,7a,8,9,10] Thus, the octahedral non-oxido-vanadium(IV) compounds such as [V(L–κ^4N,O,O,O)(acac)] and [V(L–κ^3X,O,O)$_2$] (X = S, Se) synthesized in the reaction of [VO(acac)$_2$] with appropriate ligand precursors have been structurally characterized,[7,8] other non-oxidovanadium(IV) six-coordinated compounds, [VCl_2L_4] and [VBr_2L_4] with L_4 = 4O or 2N2O donors provided by beta-diketones and Schiff bases, respectively, have been identified and studied in-detail by EPR spectroscopy by one of us. [7a] The final reaction most likely includes the oxidation of a second oxidovanadium(IV) **4** or **6** molecule of by A to form an oxidovanadium(V) (B) cation and a neutral non–oxidovanadium(III) [V($L^{2,4}\kappa^4$ONNO)(acac)] (**1** or **2**) complex as the only isolable product. The proposition of such a course is justified by the acid-induced disproportionation of the oxidovanadium(V) salen complexes showing that addition of an equimolar quantity of CF_3SO_3H to solutions of [V^{IV}O(salen)] compounds in anhydrous CH_3CN generates [V^{V}O(salen)]$^+$, [V^{III}(salen)]$^+$ and [V^{IV}(salen)]$^+$ species. Furthermore, the measured formal potentials indicated that V^{IV}O(salen)] in the presence of acid is a stronger one–electron oxidant than [V^{V}O(salen)]$^+$.[3a,11a,b] To verify experimentally the effect of weak organic acids on the reactivity of **4** and **6** depending on the solvents polarity, the reaction of these complexes with $H_2L^{2,4}$ and Hacac at a molar ratio 1 : 2 : 1, either in toluene (and n-hexane) or in CH_3CN (and ethanol) were carried out (Experimental Section). As a result, the formation of **1** and **2** in toluene or n-hexane was confirmed, whereas the compounds **4** and **6** in CH_3CN or ethanol remained unchanged. Hence, $H_2L^{2,4}$ together with Hacac provide a sufficiently acidic medium to stimulate the acid–induced disproportionation of **4** and **6** in toluene (or in n-hexane) to **1** and **2**, respectively. This is consistent with phenol acidity increase in non-polar solvents.[11c, d] Additional acidity is generated by the enol form of Hacac which is dominant in non-polar solvents[11d]. It should be emphasized that the salen–based non–oxidovanadium(III) compounds are formed in anhydrous CH_3CN but only after acidification by CF_3SO_3H,[3a] which is a considerably stronger acid (pKa ~ –15) than Hacac and phenol ligands (pKa ~9). It was postulated in our previous report that the lack of substituents at the ortho positions of the salan ligands is responsible for the unprecedented reduction of the salan–based oxidovanadium(V) compounds by NH_2NMePh to oxidovanadium(IV) ones and for the oxidation of NH_2NMePh to PhMeN–N=N–NMePh (2–tetrazene).[5a]

The aim of our new research was, among others, to find new synthetic routes to the dimeric oxidovanadium(IV) complexes with salan. We expected that ortho substituents (Me, Br) in salan $L^{4,5}$ ligands would protect their non-oxidovanadium(V) compounds from reduction by NH_2NMePh because of the V_2-μ-N-NMePh intermediate formation, according to *Method* B. However it appeared now that the reactions of [V^{V}O($L^{4,5}$–κ^4ONNO)(OPr)], (generated *in situ* with NH_2NMe_2) produced monomeric oxidovanadium(IV) compounds **6** and **7** but with no evidence of the intermediate V_2-μ-N-NMePh species. Although the ortho substituted $L^{4,5}$ ligands did not protect the oxidovanadium(V) center against reduction, they significantly prevented **6** and **7** from dimerization, opposite to **3-5** with the para–substituted $L^{1–3}$ ligands which created a mixture of monomeric and dimeric compounds.

Descriptions of Structures. Single crystals suitable for X–ray studies of the non–oxidovanadium(III) compounds **1** and **2**·0.25CH3CN and oxidovanadium(IV) **3**, **4**·2CH3CN, **5**·2CH3CN and **6**; were obtained. Their crystal data are given in Table S1. Selected bond lengths and angles for **1**, **2**·0.25CH3CN and **3**, **4**·2CH3CN, **5**·2CH3CN, **6** are collected in Tables S2 and S3, respectively. The perspective views of molecules **2** and **4** are shown in Figure 1 and Figure 2a, respectively.

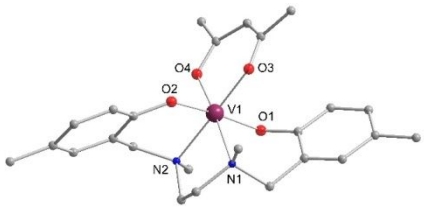

Figure 1. The molecular structure of **1** with crystallographic numbering of the donor atoms. Hydrogen atoms have been omitted for clarity.

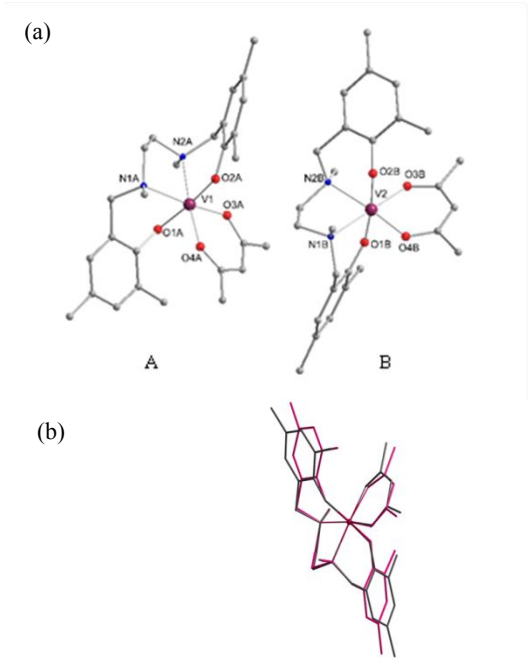

Figure 2. (a) The molecular structure of two independent molecules found in the crystal of **2**·0.25CH_3CN with crystallographic numbering of the donor atoms. Hydrogen atoms and CH_3CN molecule of crystallization are omitted for clarity. (b) Overlay of the molecular structures of molecules **A** (marked red lines) and **B** (marked by gray lines). The molecules were aligned by pairs of atoms: V1 and V2, O1A and O2B, as well as N1A and N2B.

Compounds **1** and **2** crystallize as monomeric molecules and exhibit *cis*–α geometry with the oxygen donors of the $(acac)^-$ group and the amine nitrogen atoms of the $L^{2,4}$ ligands occupying mutually *cis* coordination sites. The two aryloxido oxygen donors coordinate in a *trans* fashion. This geometry is not surprising since the most structurally characterized salan–metal coordination compounds are *cis*–α.[1c,3d,4b,5a,5c,13,14] To our knowledge, compounds **1** and **2** are the first examples of structurally characterized salan–based non–oxidovanadium(III) compounds. In **2**, there are two independent molecules **A** and **B** in the asymmetric unit (Figure 2a) with slightly different structural parameters as indicated by the overlay of molecules A and B depicted in Figure 2b. The crystal packing of **2** clearly indicates the influence of the intermolecular interactions such as hydrogen bonding and C–H···π contacts on the actual structural parameters of molecules A and B (Figure S2 and S3; Table S4 and S5). As a consequence, the relevant bond lengths V–O, V–N and angles vary over the range of 0.02–0.04 Å and 5–10°, respectively (see Table S2). Nevertheless, V–O and V–N bond lengths of the $L^{2,4}$ ligands (av. 1.93 Å and av. 2.20 Å, respectively) as well as the V–O distances of the $(acac)^-$ group (av. 1.99 Å) in **2** and **4** are, within statistical error, in agreement with those observed for $[V(L–\kappa^4O,N,N,O)(acac)]$ {L = $[Me_2NCH_2CH_2N(CH_2–4,6–Me_2–C_6H_2O)_2]^{2-}$}, containing the tripodal isomer of the linear L^4 ligand.[15a]

In **1**, the molecules interact *via* C24–H24C···O1^{i} ([i] x, 1/2–y, 1/2+z) hydrogen bonds forming chains that stretch along [001] direction (Figure S1, Table S6). Within the chains C–H···π interactions between neighboring molecules of **1** are also observed (Table S7). In **2**, molecules interact *via* hydrogen bonds of C23B–H23D···O1A^{ii} (ii = 1/2–x,–1/2+y,1/2–z) either within the chains or layers (Figure S2, Table S4) and C–H···π intermolecular interactions within the chains are observed (Figure S3, Table S5).

In the solid state, the dimeric molecules **3**–**5** are very similar, and are exemplified by **4** in Figure 3 (the molecular structure for **3**, Figure S4; for **5**, Figure S7). Selected bond distances and angles for **3**–**5** are collected in Table S3. As far as we are aware, these are the first dimeric oxidovanadium(IV) salan–based compounds to be structurally characterized. The central, planar or nearly planar four–membered ring is composed of two vanadium atoms and two bridging oxygen atoms (O3) of the $L^{1–3}$ ligands. The geometry about each vanadium atom is distorted octahedral with three oxygen atoms (the oxido O2 and two aryloxido O1, O3 of the $L^{1–3}$ ligands) and one nitrogen (N1) of the $L^{1–3}$ ligands in the equatorial positions and the second nitrogen (N2) atom of the $L^{1–3}$ ligands and oxido group occupying the axial sites. As is the case in **1** and **2**, the molecules **3**–**5** exhibit *cis*–α geometry. The V–$O_{aryloxido}$, V–O_{oxido} and V–N bond lengths in **3**–**5** are statistically very similar. A significant difference is observed for the V–O1 and V–O3 distances (av. 1.921 and 2.019 Å, respectively) as a consequence of the bridging role of the V–O3 oxygen, whereas the V–N2 bond lengths are significantly longer than the V–N1 as a result of stronger *trans* interaction of the N2 nitrogen with the $O2_{oxido}$ atom.[15b]

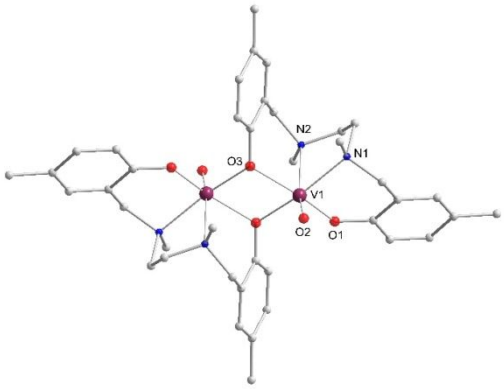

Figure 3. The centrosymmetric structure of **4**·2CH_3CN with crystallographic numbering of the donor atoms. Hydrogen atoms and CH_3CN molecules of crystallization have been omitted for clarity.

For **3**, **4** and **5** the layered architectures were also considered. Their layers parallel to the (010) plane are shown in Figures S5, S6 and S8, respectively. The chains of molecules of **3**, **4** and **5** are held together by C parallel H···π interactions (Table S8, S9 and S11, respectively). In the case of **4** and **5**, molecules of CH_3CN located between the layers are involved in C7–H7A···N1X hydrogen bonds (Table S10 and S12, respectively).
In contrast to the dimeric nature of **3**–**5**, the X–ray study of **6** revealed its mononuclear structure. Its molecular structure is shown in Figure 4, and selected bond lengths and angles are collected in Table S3.

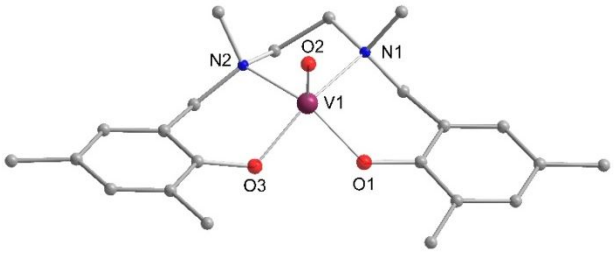

Figure 4. The molecular structure of **6** with crystallographic numbering of the donor atoms. Hydrogen atoms have been omitted for clarity.

The coordination environment around the vanadium atom is a distorted square pyramid (trigonality index[15c] τ = 0.17) with the O_2N_2 set of atoms from the L^4 ligand in the equatorial plane and the oxido group (O2) in an axial position. The $O_2N_{2\ atom}$ set of atoms is significantly distorted from a planar geometry; the vanadium atom is pulled out of the mean equatorial plane by 0.59(2) Å towards the oxido group. The distortion is best illustrated by the variation of the N1–V–O3 and N2–V–O1 angles of 151.13(7) and 140.81(3)°, respectively. Similar structural parameters were observed for the monomeric [VO(L^1–κ^4O,N,N,O)]·EtOH.[5a] The V–$O2_{oxido}$ distance of 1.602 (9) Å is statistically similar to that found in [VO(L^1–κ^4O,N,N,O)] (1.592(1) Å) and is typical for five–coordinate vanadyl species.[16] Both the V–$O_{aryloxido}$ or V–N bond lengths are unequal [V–O1, 1.898(1) Å; V–O3, 1.922(1) Å and V–N1, 2.200(9) Å; V–N2, 2.167(9) Å] as a consequence of geometric distortion around the vanadium center. Additionally, the V–$O_{aryloxido}$ distances are shorter (~0.03 Å) than those observed for monomeric [VO(μ–L^1–κ^4O,N,N,O)]·EtOH, in which corresponding distances are probably lengthened by an intermolecular hydrogen–bond interaction with EtOH molecule.[5a] The packing diagram for **6** viewed down the [010] direction is shown in Figure S10. The crystal structure of **6** exhibits layers parallel to the [010] plane. The adjacent molecules of **6** contact each other via C–H···π and π···π interactions (Figure S11, Table S13 and S14).
Compound **6** is the second example of a structurally characterized oxidovanadium(IV) compound bearing the salan ligand.

EPR Spectroscopy.

The EPR spectra were interpreted in terms of the standard spin Hamiltonian:

$$\hat{\mathbf{H}} = \mu_B \mathbf{B}\{\mathbf{g}\}\hat{\mathbf{S}} + D\left\{\hat{\mathbf{S}}_z^2 - \frac{1}{3}S(S+1)\right\} + E\left(\hat{\mathbf{S}}_x^2 - \hat{\mathbf{S}}_y^2\right) + \hat{\mathbf{S}}\{\boldsymbol{A}\}\hat{\mathbf{I}} \quad (1)$$

The spin Hamiltonian was modified for particular cases: The hyperfine term $\hat{\mathbf{S}}\{\boldsymbol{A}\}\hat{\mathbf{I}}$ was omitted for the monomeric V(III) compounds **1** and **2**, which exhibited no hyperfine structure. The zero–field splitting terms with *D* and *E* are not applicable to the monomeric V(IV) compounds with electronic spin S = $^1/_2$ and were removed.

The V(III) Compounds. Compounds **2,4** are silent in X–band EPR, as expected for V(III) in low symmetry environment.[17] High–Field EPR measurements were thus performed for **1** and **2**, spectra of which are compared in Figure 5.

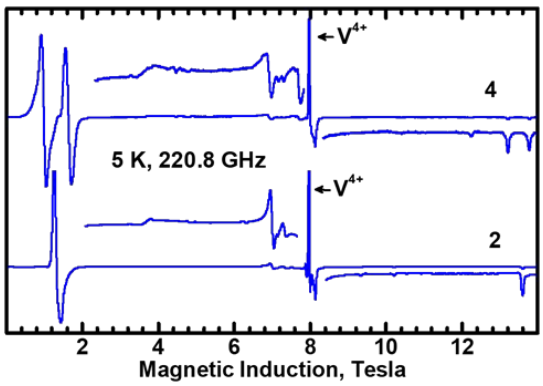

Figure 5. HFEPR spectra of **1** and **2** recorded at conditions indicated.

It is interesting that compound **2** contains two slightly different molecules as is shown in Figure 2b and exhibits two distinct EPR spectra (Figure 5) which is a very rare case. The resolution was sufficient to determine the spin Hamiltonian parameters of each species.
To determine the spin Hamiltonian parameters accurately, a large number of spectra were recorded at various frequencies (like those presented in Figure 6) and the positions of the canonical transitions, that is those occurring at the molecular X, Y or Z orientations, were fitted (Figure 7). A similar procedure applied to **2** resulted in determination of the spin Hamiltonian parameters for two crystallographically independent molecules present in the structure. The parameters are given in the Figure 8 caption.

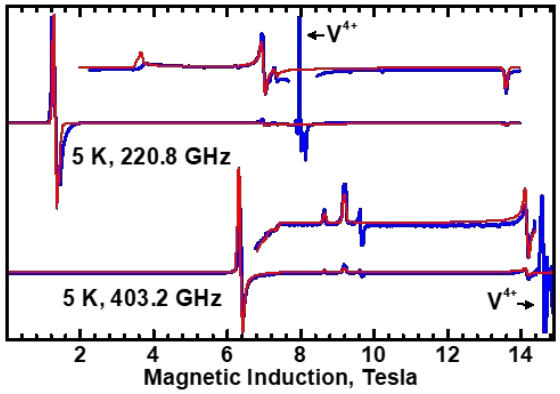

Figure 6. HFEPR spectra of **1**. Blue: experimental. Red: simulated with parameters in Fig. 7 caption.

An important advantage of the HFEPR is the possibility of determination of the sign of the zero–field splitting parameters *D* and *E*. Although the positions of the EPR resonances do not depend on the sign of *D* or *E*, the intensity pattern in the low–temperature spectra depends on these signs. This effect relies on the magnitude of the Zeeman energy being comparable to the thermal energy, *kT*, and not on the magnitude of *D*. Accordingly, the sign of a very small $|D|$ can also be determined. Compound **1** as well as both species in **4** **2** have large positive *D* over the range 5.1 – 5.4 cm^{-1} and large *E*, close to *D*/3.

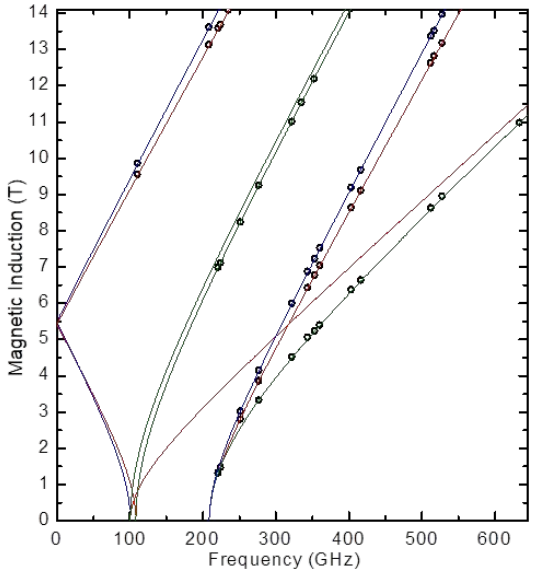

Figure 7. Frequency dependencies of the resonances observed in **1**. Black circles are the experimental points. The green, blue and red lines were calculated at the molecular orientations X, Y and Z, respectively using the best–fit parameters g_x = 1.946(2), g_y = 1.885(1), g_z = 1.978(1), *D* = 5.288(4) cm^{-1}, *E* = 1.679(3) cm^{-1}.

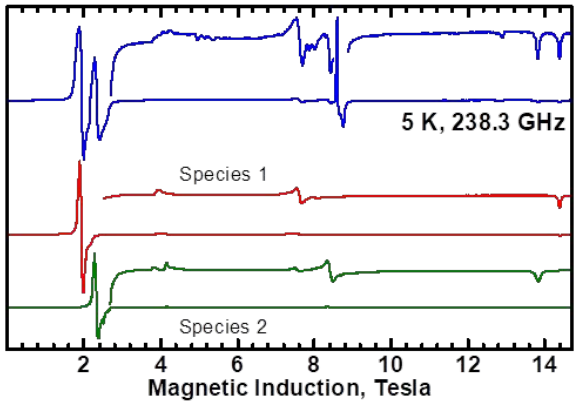

Figure 8. HF EPR spectra of **2.** Blue: experimental. Red: simulated for species 1 with g_x = 1.946(6), g_y = 1.889(3), g_z = 1.974(3), *D* = 5.41(1) cm^{-1}, *E* = 1.69(1) cm^{-1}. Green: simulated for species 2 with g_x = 1.85(1), g_y = 1.922(3), g_z = 2.005(5), *D* = 5.115(8) cm^{-1}, *E* = 1.662(4) cm^{-1}.

Dimeric V(IV) Compounds. The powder X–band EPR spectra of binuclear compounds 3–5 shown in Figure 9, exhibit intense central and weaker half field (~1600 G) lines associated with the allowed (ΔMs = 1) and forbidden (ΔMs = 2) resonance transitions, respectively which occur within the spin triplet state (S = 1). The triplet state arises from the exchange coupling of two V^{4+} ions, each bearing one unpaired electron. The V(IV) dimers studied here are not easy to study in HFEPR because of their very small zero–field splitting which at high frequencies becomes comparable to the splitting due to the *g* anisotropy. Also, the linewidth increases compared to the X–band spectra owing to the *g*–strain causing disappearance of the hyperfine structure. Nevertheless, the HFEPR spectra of **4** (Figure 10) allowed refine the *g* values and determine that *D* and *E* are positive.

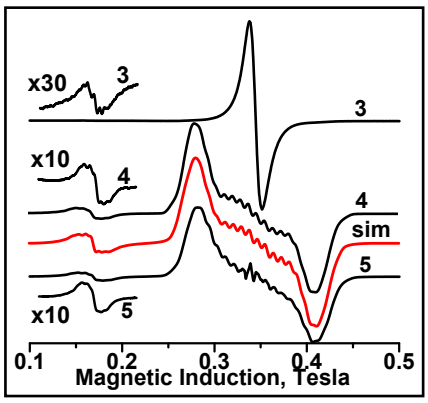

Figure 9. The X–band EPR spectra of 3–5 at 77 K. The red trace (sim) was simulated with spin Hamiltonian parameters given in the text. The signals due to forbidden ΔMs = 2 transitions at about 1600 G are also shown at increased amplification.

The X–band spectra reveal also a hyperfine splitting of the ΔMs = 1 and ΔM_s = 2 lines for **4** and **5** and ΔM_s = 2 line for **3** due to coupling of the electron spins with nuclear spins (*I* (^{51}V) = 7/2) of two vanadium atoms. The observed fifteen–line pattern of hyperfine splitting provides an unambiguous proof

of magnetic interaction between two V(IV) centers leading to S = 1.

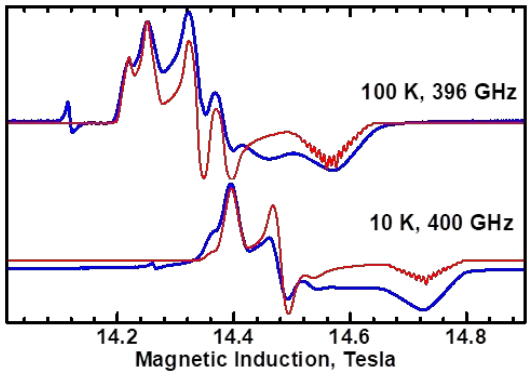

Figure 10. HF EPR spectra of **4**. The parallel part was simulated with a too small linewidth to show the internal structure of the band. A narrow resonance at 14.1 T (top) and at 14.27 T (bottom) is due to a trace amount of a free–radical contamination (g = 2.0037).

The lack of the lines assigned to $\Delta M_s = 1$ electron transitions in the spectrum **3**, together with the need for much greater gain to observe the forbidden $\Delta M_s = 2$ line than for **4** and **5**, indicate a substantial content of monomeric form in **3**, greater than in **4** and **5**. Simulation of the experimental spin–triplet spectra for **4** and **5,** aided by the HFEPR, allowed determination of the spin Hamiltonian parameters: $g_x = 1.981$, $g_x = 1.976$, $g_z = 1.942$, $D = 0.007$ cm^{-1}, $E = 0.039$ cm^{-1}, $A_x = 23\cdot10^{-4}$ cm^{-1}, $A_y = 27\cdot10^{-4}$ cm^{-1}, $A_z = 79\cdot10^{-4}$ cm^{-1}. The parameters are similar to those obtained previously for the same dimeric oxidovanadium(IV) compounds prepared by us previously by reducing the appropriate oxidovanadium(V)–salan compounds using NH_2NMePh.[5a] It is especially noteworthy that the spectra of the oxidovanadium(IV) dimers studied here could only be simulated with the E parameters (the measure of rhombicity of ZFS) much larger than *D* (axial component of *ZFS*). This relation was observed firstly for the oxidovanadium(IV) dimer with N, N',N''–trimethyl–1,4,7–triazacyclononane ligands and bis(μ–hydroxo) bridge implying that the central part of the "allowed" signal corresponds to the parallel orientation.[18] The value of A_z component ($79\cdot10^{-4}$ cm^{-1}) of hyperfine coupling tensor A equals half of that determined for monomeric VO^{2+} compounds, which is expected for the binuclear compounds.[19] As normally one finds the *D* and *E* parameters obeying the convention $|E| < |D|/3$, a comment will be useful here. The non–conventional set of *D* and *E* indicates that the "distinguished" component (that is a component different from the remaining two ones, which are similar to each other) of the zero–field splitting tensor is not parallel to g_z. The g_z component in vanadyl systems is directed roughly towards the axial oxygen atom. The zero–field splitting in a dimeric compound contains the spin–orbit coupling related contribution (also referred to as anisotropic exchange interactions) and the magnetic dipole–dipole contribution. The former one is a major part of the zfs in copper(II) dimeric compounds, in which its distinguished component D^{ex}_{zz} is parallel to g_z.[20] The largest component of the dipole–dipole related zfs contribution is directed along the metal–metal vector. For example, in some copper dimers containing a CuOOCu dibridged unit, similar to the one in our V dimers, the anisotropic exchange contribution, D^{ex} of about –1 cm^{-1} was found, while the dipolar contribution was –0.07 cm^{-1}. [21] The theory of anisotropic exchange is presented in reference 20. The formulas for the spin–orbit coupling related parts of the zero–field splitting, D^{ex} and E^{ex} presented in that paper, can be adapted to V^{4+}:

$$D^{ex} = 2\frac{\xi^2 J_{xy,x^2-y^2}}{\Delta E^2_{xy,x^2-y^2}} - \frac{1\xi^2 J_{xy,yz}}{4\Delta E^2_{xy,yz}} - \frac{1\xi^2 J_{xy,xz}}{4\Delta E^2_{xy,xz}} \qquad (2)$$

$$E^{ex} = \frac{1\xi^2 J_{xy,yz}}{4\Delta E^2_{xy,yz}} - \frac{1\xi^2 J_{xy,xz}}{4\Delta E^2_{xy,xz}} \qquad (3)$$

where ξ is the spin–orbit coupling constant (250 cm^{-1} for V^{4+}, 828 cm^{-1} for Cu^{2+}),[22] the quantities $J_{xy,xz}$ etc. are exchange integrals in the excited states of a dimer, in which one V^{4+} is in its ground state d_{xy}, while another one is in an excited state. $\Delta E_{xy,xz}$ etc. are the ligand–field splittings between the ground state and an excited state of a single ion. Because the terms in equations above appear in the theory of the *g* factor, D^{ex} and E^{ex} may also be expressed using the deviations $\Delta g_i = g_i - g_e$, of the *g* components from the free–electron g_e=2.0023:

$$D^{ex} = \frac{1}{32}\Delta g_z^2 J_{xy,x^2-y^2} - \frac{1}{16}\Delta g_x^2 J_{xy,yz} - \frac{1}{16}\Delta g_y^2 J_{xy,xz} \qquad (4)$$

As the Δg_i values are much smaller in V^{4+} than in Cu^{2+}, it becomes clear that in dimers with similar MOOM bridge arrangements, the zero–field splitting may be dominated by the anisotropic exchange in dinuclear Cu(II), but not in V(IV) complexes. In the latter ones, the magnetic dipolar contribution becomes larger than the exchange related contribution. The dipole–dipole related part of *D* may be estimated from

$$D^{dipole} = -\frac{3g^2\mu_B^2}{2R^3_{V-V}} \qquad (5)$$

With R_{V-V} of 3.25 Å one obtains D^{dipole} of –0.075 cm^{-1}, while E^{dipole} = 0. D^{dipole} and E^{dipole} are expressed in a system of coordinates in which the Z axis is along the V–V direction, but the directions of the axes of the exchange–related zero–field splitting tensor are expected to be parallel to the axes of *g*. The g_z direction is roughly perpendicular to V–V. Converting the D^{dipole} and E^{dipole} to the coordinates of *g* (by swapping the Y and Z axes), one obtains D^{dipole} = 0.0375 cm^{-1} and E^{dipole} = 0.0375 cm^{-1}. Now, the D^{ex} and E^{ex} can be calculated by subtracting from the experimental *D* and *E* values these latter numbers, to obtain D^{ex} = –0.030 cm^{-1} and E^{ex} = 0.0015 cm^{-1}. Interestingly, the exchange–related zero–field splitting is close to being axial ($|E^{ex}|$ small compared to $|D^{ex}|$). For comparison, in compounds with CuOOCu bridge units, D^{ex} is some 33 times larger.[21]

Frozen solution EPR spectra of the dimeric compounds **3**–**5** in CH_3CN and **4** in CH_2Cl_2 (Figure S12) show eight hyperfine lines at both parallel and perpendicular orientations proving the interaction of *S* = 1/2 with the nucleus spin of one vanadium and hence the formation of mononuclear compounds. Only for

4 in CH_2Cl_2 solution at increased amplification, a weak forbidden line is observed due to the S = 1 state. That transition exhibits hyperfine splitting of two vanadium nuclei. The frozen solution spectra of the monomeric compounds **6** and **7** in CH_2Cl_2 are similar to those for the monomers formed from dimeric compounds **3**–**5** in solutions. The spectra of all these monomeric compounds may be simulated using the same spin Hamiltonian parameters $g_x = g_y$ =1.979, g_z = 1.947, $A_x = A_y = 55 \cdot 10^{-4}$ cm^{-1}, $A_z = 163 \cdot 10^{-4}$ cm^{-1}, which are typical for oxidovanadium(IV) compounds with the N_2O_2 ligand donor set in the *xy* plane.[23] This is in agreement with the X–ray structure of **6** and also suggests that the molecular structure of **7**, of which no crystals were obtained, is similar to that of **6**.

Magnetic Properties.

Dimeric V(IV) Compounds.

As will be shown below, the metal-metal interactions in compounds **3–5** are surprisingly ferromagnetic in contrast with the strong antiferromagnetic coupling typically reported in literature for such kind of complexes.[24] Magnetic data were analyzed taking into account the presence of monomeric counterparts of dimers **3–5** (see Scheme 1) in our samples, which was confirmed by EPR spectra. The molar magnetic susceptibility for dimeric oxidovanadium compounds **3**–**5** has been converted to the $\chi_M T$ product whose temperature dependence is displayed in Figure 11. The values of $\chi_M T$ at room temperature 1.16 cm^{3}mol^{-1}K (3.05 μ_B) for **3**, 0.94 cm^{3}mol^{-1}K (2.96 μ_B) for **4** and 0.66 cm^{3}mol^{-1}K (2.30 μ_B) for **5** are higher (**3** and **4)** and somewhat lower (**5)** than expected 0.72 cm^{3}mol^{-1}K (μ_{eff} = 2.41 μ_B) for two V(IV) ions without any exchange interactions; with $S = {}^1/_2$ and g_{av} = 1.97 taken from EPR. The three dimeric compounds exhibit weak ferromagnetic coupling whose strength increases in the series **3–5–4** (Figure 11), which can be seen from the shift of the maximum χT towards higher temperature and increasing height of that maximum.

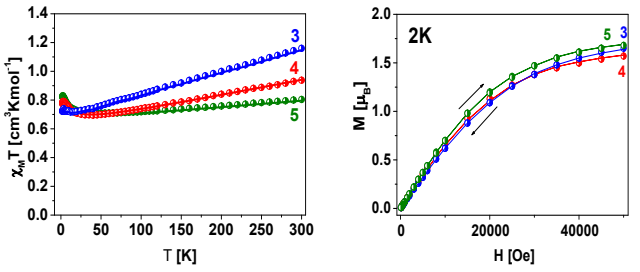

Figure 11. DC magnetic data for **3**–**5**. Left – (◔) temperature dependence of χ_MT. Right – field dependence of the magnetization per formula unit. The solid lines (on both graphs) are calculated using the HDVV spin Hamiltonian and PHI program.[25]

A significant contribution of the temperature independent paramagnetism (TIP) is reflected in the slopes of the $\chi_M T$ dependencies at higher temperatures. The exchange interaction between two V(IV) ions ($S_A = S_B$ = ½) in **3–5** was described using a model of binuclear units coupled through an aryloxido bridge. Various additional V···V intermolecular interactions transmitted through the hydrogen bonds are described by the effective *zJ'* parameter (where z is the number of adjacent binuclear or paramagnetic species around a given binuclear unit). The calculations were based on the Heisenberg–Dirac–Van Vleck Hamiltonian in zero field given by eq. (6)

$$\hat{H} = -J\,\hat{S}_A\hat{S}_B - zJ' \langle S_z \rangle \hat{S}_z \qquad (6)$$

describing the isotropic exchange interaction, ferromagnetic for $J > 0$. The well–known PHI program,[25] was used which allows for the simultaneous fitting of $\chi T(T)$ and $M(\mu_0 H)$ dependencies. The temperature independent paramagnetism (TIP) and the fraction of monomeric counterparts of dimeric compounds being in equilibrium according to the EPR spectra (x = 1 for one uncoupled spin) were also included into the fitting procedure. The best agreement with the experimental magnetic data for **3–5** was obtained with g = 1.968, J = 0.40 cm^{-1}, zJ' = –0.01 cm^{-1}, $TIP = 218 \cdot 10^{-5}$, x = 0.25, $R = \Sigma[(\chi T)\text{exp} - (\chi T)\text{calc}]^2 / \Sigma[(\chi T)\text{exp}]^2 = 1.84 \cdot 10^{-5}$ (lines in Figure 11, left) for **3**; g = 1.97, J = 5.34 cm^{-1}, zJ' = –0.2 cm^{-1}, x = 0.33, $TIP = 159 \cdot 10^{-5}$, $R = 7.37 \cdot 10^{-6}$ for **4** and with J = 3.22 cm^{-1}, zJ' = 0.01 cm^{-1}, g = 1.96, $TIP = 599 \cdot 10^{-6}$, x = 0.21 and $R = 7.04 \cdot 10^{-7}$ for **5**. The g–values are close to those obtained by simulation of the EPR spectra. The temperature independent paramagnetic term is bigger than usually found.[2e] ~~We cannot offer an explanation but this was confirmed by repeated measurements.~~ Although the origins of the observed phenomenon are unclear, it was verified by repeated measurements. Because of that, TIP was subtracted from the experimental data in Figure S13 for a better presentation. The PHI program assumes that a monomeric contamination is a species with g=2 and TIP=0. The entire observed TIP is thus ascribed to a dimer, but the contamination here is a monomer of V(IV) whose TIP should be close to half of the dimer TIP. Thus, when applying this method to a situation where the fraction of monomer is as large as ~0.33 (like in **4**), the dimer TIP is obtained too high by a factor of 1.5. It must be emphasized that the synthetic method used in this work produces by its nature a mixture of the dimeric and monomeric species with a considerable fraction of the latter. The variation of magnetization versus magnetic field at 2 K (Figure 11, right) clearly confirms that S=1 is the ground state in dimers **3–5**. Secondly, the magnitude of zJ' demonstrates that the inter–dimer interactions are not negligible.

~~Although~~ The explanation of these unexpected ferromagnetic properties does not fit into the theories presented so far. According to Plass's classification,[2c] compounds **3–5** present an anti–orthogonal configuration in relation to the orientation of the V=O group with respect to the plane defined by the two vanadium centers and two bridging oxygen atoms for which a direct strong antiferromagnetic interaction or superexchange mechanism between the d_{xy} magnetic orbitals could be expected (Figure S14). For example, the binuclear octahedral oxidovanadium(IV) compounds with aryloxido, alkoxido and hydroxido bridging ligands show strong antiferromagnetic feature (with J from –168 to –354 cm^{-1}) (Table S15).[24] Ceccato et. al. have stated that the J values for those series of compounds are independent of the V–O–V angle, and the V···V

and V–μ–O distances, and inferred that the dihedral angle (τ) between the equatorial planes, has a decisive impact on the nature and strength of the magnetic interactions (Table S15).[24a] The highest antiferromagnetic *J* values were observed for compounds with the anti– and syn–orthogonal configurations having τ in a range 180–131.1°.[24a] Although the τ values are 180° or slightly less in compounds **3–5** (Figure S14), they exhibit weak ferromagnetic exchange interactions (*J* is in a range +0.40 to +5.34 cm^{-1}) similar to those for $[(VO)_2(HL_2)_2]\cdot MeOH$ {H_3L = N–salicylidene–2–[bis(2–hydroxyethyl)amino ethylamine}[2c] having anti–coplanar configuration, *J* = +3.1 cm^{-1} and τ = 0. In our opinion, the influence of the value of V–O–V angle as well as the V···V and V–μ–O distances on the magnitude of magnetic interactions cannot be ignored. The much longer V···V distance and larger V–O–V angle in **3–5** than those in analysed by Ceccato et. al compounds[24a] reduce the overlap between the MO's bearing unpaired electron resulting in reduction of the magnitude of magnetic coupling. Moreover, the strength of the intermolecular interaction (*zJ'*) in **4** indicate the importance of secondary exchange pathways which involve the C–H···Cg (π–ring) contacts within the material (Figure S9).

Broken Symmetry calculations of *J* in the dimeric compounds.

Broken symmetry calculations[26-28] were performed for compounds **3**, **4** and **5** to evaluate the expected magnitude of the exchange integral. In this method, two SCF calculations are performed: in one, the spins on the interacting atoms are assumed parallel and in the second one they are assumed antiparallel, which is referred to as a broken symmetry state. The *J* value is subsequently evaluated from the energy difference between the high–spin state and the broken symmetry state,

$$J=2(E_{HS}-E_{BS})/[S_{HS}(S_{HS}+1)-S_{BS}(S_{BS}+1)]$$[29]

ORCA software package[30] was employed. Functional B3LYP/G was used with TZVPP functions for all atoms.[31-33] The calculations produced ferromagnetic *J* values of 21 cm^{-1}, 35 cm^{-1} and 29 cm^{-1} for **5**, **6** and **7**, respectively. In the experience of some of us, the method tends to produce overestimated (by some 50%) but reasonable *J* values. The decidedly too large values calculated by ORCA in our three cases are thus disappointing. For comparison, we performed a similar DFT calculation for a strongly antiferromagnetically coupled bis(*μ*–hydroxo)bis[oxo(1,4,7–triazacyclononane vanadium(IV)] dibromide, for which *J* = –354 cm^{-1} was determined from magnetic data by Wieghardt *et al*.[24d] The calculation produced *J* = –540 cm^{-1}. cm^{-1}. The striking difference between our dimers and the triazacyclononane (TCNA) compound was thus reproduced. It is known that the overlap of the magnetic orbitals containing the unpaired electrons of two interacting ions gives rise to the antiferromagnetic coupling. For **3**, 4 and **5** the overlap integrals of the magnetic orbitals (calculated by the broken symmetry procedure) were 0.027, 0.019 and 0.022, respectively, while it was equal to 0.13 for the TCNA compound. The trend of the *J* values is parallel to the trend of the overlap integrals, with the ferromagnetism increasing (or antiferromagnetism decreasing) when the overlap is reduced. The orbital overlap in **4** and in the TCNA compound is shown in Figure 12. The dramatic dependence of *J* on the orbital overlap suggests that the magnitude and sign of *J* depend on how well the d_{xy} orbitals of two V^{4+} ions are aimed at each other, and the empirical rules described above may not be perfect in predicting this, while the DFT software is successful, at least qualitatively. The very steep correlation between the orbital overlap and *J* may also be a reason for the unsatisfactory numerical values of the calculated *J* values.

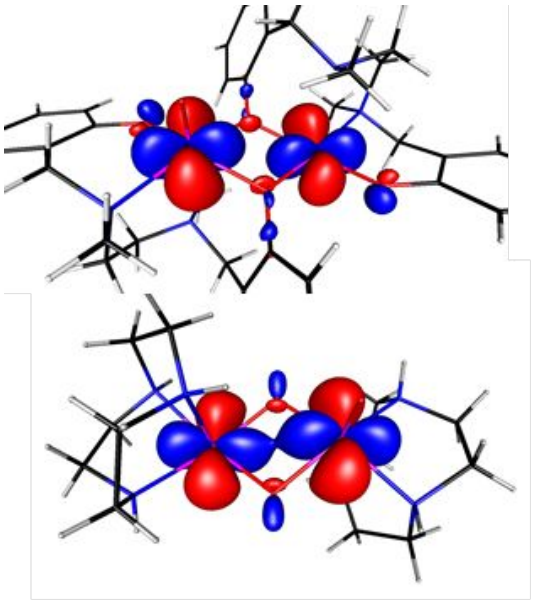

Figure 12. Overlap of the magnetic *xy* orbitals in bis(*μ*–hydroxo)bis[oxo(1,4,7–triazacyclononane vanadium(IV)] dibromide (bottom) and in **4** (with some outer parts cut off for clarity). The symmetric orbitals (thus belonging to S=0) are plotted at the isosurface value of 0.04. The Z axis is perpendicular to the VOOV bridge plane.

Monomeric V(III) and V(IV) Compounds.

Since the spin Hamiltonian parameters *g*, *D* and *E* are already known from EPR (Figure S15), the magnetic susceptibility measurements for monomeric non–oxidovanadium(III) **1**, **2** and oxidovanadium(IV) **6**, **7** appear to be superfluous, particularly because the bulk magnetic susceptibility is weakly sensitive to *D* and *E*. Nevertheless, this technique can provide information on intermolecular interactions and spin states (Figures S16 – S18).

At the room temperature, the effective magnetic moments are 2.58 μ_B and 3.02 μ_B for **1** and **2**, respectively, a little different than the expected for S = 1 (V^{3+}), nevertheless they are consistent with vanadium(III) d^2 species. Similar effective magnetic moment to **2** was observed for [V(L)(acac)] {L = $[Me_2NCH_2CH_2N(CH_2–4,6–Me_2–C_6H_2O)_2]^{2-}$} (2.91 μ_B, 295K) [15]. In the case of monomeric oxidovanadium(IV) compounds **6** and **7** the effective magnetic moments at room temperature are 1.99 μ_B and 1.84 μ_B, respectively, and are close to that expected for S = ½ spin of vanadium(IV) d^1 species. The intermolecular

interactions in all monomeric complexes was calculated according to procedure described in supplementary part. The resulting *zJ'*, –0.14 cm^{-1} for **2**, –0.01 cm^{-1} for **6**, –0.08 cm^{-1} for **7,** indicates, that a weak exchange interaction between nearest vanadium atoms in the crystal lattices can exist but in the case of **1** and **2** the zero-field splitting effect of the V^{+3} ions (D = 5.29 cm^{-1} (**1**) and D = 5.26 cm^{-1} (**2**) according to our HFEPR studies) is predominant and affects the decrease of $\chi_M T$ in the low temperature range.

Calculations of *D* in 5. In recent years, Density Functional Theory (DFT) and *ab initio* methods have been applied to get insight into the nature of the zero–field splitting.[34,35] We have attempted to calculate the spin–orbit coupling contribution to D and E in our compound **5** by using the state–averaged complete active space self–consistent field (CASSCF)[34,35] approach, with 2 electrons in 5 orbitals. 10 triplet states have been taken into account. Similarly to our broken symmetry calculations above, the functional B3LYP was used with def–2 TZVPP functions[36] for all atoms. The calculations produced D = –10.0 cm^{-1}, E/D = 0.19. The result is thus disappointing, as the experimental data are D = +5.29 cm^{-1} and E/D = 0.31. The sign of D is difficult to determine theoretically when the E/D ratio is high. With the „maximum rhombicity", that is E/D = 1/3, the diagonalized traceless zero-field splitting tensor has three components, D_{xx} = 0, D_{yy} = – (2/3)D and D_{zz} = (2/3)D and powder EPR spectra simulated with either negative or positive D will be identical, even at the lowest temperatures. With $|E/D|$ slightly smaller than 1/3, the sign of D depends on a small deviation of D_{xx} towards either D_{yy} or D_{zz}, the calculation of which may well be beyond the accuracy of theoretical methods. The wrong sign of D obtained from CASSCF is thus not necessarily worrisome, while the absolute magnitude of D still is. Large differences between the theoretically calculated[37a] and experimental[37b] D parameters for V(III) complexes were also obtained by others. It should be emphasized that the sign of D can be determined experimentally by HFEPR even at E/D ratios close (but not equal) to 1/3, provided that the Y and Z transitions are spectrally resolved, as is the case here.

.

Conclusions

In conclusion, the vanadium compounds of the salan ligands containing either para or para and ortho substituents on the aromatic rings are presented. Two synthetic methodologies were used to obtain oxidovanadium(IV) compounds. The first is a high-yield reduction of appropriate oxidovanadium(V) precursors by NH_2Me_2 in CH_3CN to obtain **6** and **7**. The second route involving reactions of $[VO(acac)_2$ with $H_2L^{1–5}$ in CH_3CN or EtOH, is admittedly less efficient but capable of obtaining compounds **3**–**6** in a crystalline form. The use of toluene or *n*–hexane instead of CH_3CN for the latter reactions resulted in the formation of non–oxidovanadium(III) compounds **1** and **2**. It has been proved that H^+ eliminated from $H_2L^{2,4}$ generates a sufficiently acidic medium in toluene or *n*–hexane to stimulate the acid–induced disproportionation of **4** and **6** and is responsible for their reduction to **1** and **2**. Compounds **1**, **2** and **3**–**5** are the first examples of structurally characterized non–oxidovanadium(III) and dimeric oxidovanadium(IV) salan–based species. The structures of the oxidovanadium(IV) compounds were found to be controlled by the substituent position in aromatic rings at the salan ligands as well as by the solvent. The $L^{4,5}$ ligands substituted at ortho positions (besides para) generate monomeric oxidovanadium(IV) (**6** and **7**) compounds, whereas the $L^{1–3}$ ligands substituted at para positions, favor the formation of a mixture of dimeric and monomeric forms (**3**–**5**) in the solid state, while in solution the monomeric molecules dominate. Furthermore, the para substitution of $L^{4,5}$ ligands do not protect the vanadium(V) in oxidovanadium(V) compounds against reduction by substituted hydrazine, but significantly prevent dimerization of monomeric $[VO(L^{4,5}–\kappa^4ONNO)]$ species.

The comprehensive analysis of HFEPR spectra proved that metal centers in **1** and **2** are the V(III) (S = 1) ions in low symmetry coordination as indicated by the characteristic zero–field splitting parameters D and E in the range 5.1–5.4 cm^{-1} and 1.66–1.69 cm^{-1}, respectively. The presence of two slightly different molecules in the crystal structure of **2** resulted in rare observation of two distinct HFEPR spectra with slightly differing parameters. The X–band and HFEPR spectra confirmed the dimeric structure of the V(IV) compounds **3**–**5**, the spectra of which are characteristic of S = 1 with hyperfine splitting due to two V(IV) nuclei and an unusual $|E| > |D|/3$ relation, which could be explained. Magnetic measurements have shown that compounds **3** – **5** are rare examples of dimeric forms of oxidovanadium(IV) with unusual, weak ferromagnetic interactions in contrast to the strong antiferromagnetic expected for the anti-orthogonal configuration. These results have been confirmed also by the theoretical calculations.

Experimental

Materials and methods

Caution! 1,1–Dimethylhydrazine is an acutely toxic material. It can cause burns to the skin, eyes and is highly irritating to the mucous membranes. All operations should be conducted in a well–ventilated fume hood and behind a safety shield.

All operations were carried out under a dry dinitrogen atmosphere, using the standard Schlenk techniques. All solvents were distilled under dinitrogen using appropriate drying agents. Reagents were purchased from the Aldrich Chemical Co. and used without further purification unless stated otherwise. Ligand precursors $H_2L^{1–5}$ were conducted through procedures previously described.[4b,5a,13,37,38]

Synthesis

[V^{III}(L2,4–κ4O,N,N,O)(acac)] (1, 2). ***Method 1***. To a solution of ligand precursors $H_2L^{2,4}$ in toluene or n-hexane [$V^{IV}O(acac)_2$] was added (1 : 1 ratio) and a blue–green mixture was refluxed for about 15 h (toluene) or 3 days (n-hexane) resulting in a brown solution or a light-brown solid, respectively. In case of toluene post-reaction mixture, all volatiles were removed *in vacuo* to dryness to yield dark–orange products which were washed with n–hexane and dried under vacuum. Diffraction–quality bright–orange crystals of **1** and **2**·0.25CH_3CN were obtained by recrystallizing from toluene and acetonitrile, respectively, at room temperature. Crystals of 1 and 2 were characterized as follows:

1: Yield: 53%. Calcd for $C_{25}H_{33}N_2O_4V$: C 63.00, H 6.98, N 5.88. Found: C 62.87, H 6.89, N 5.81%. μ_{eff} = 2.58 μ_B (300 K).

2·0.25CH_3CN: Yield: 49.5%. Calcd for $C_{27}H_{37}N_2O_4V$·0.25CH_3CN ($C_{27.5}H_{37.75}N_{2.25}O_4V$): C 64.26, H 7.40, N 5.55. Found: C 64.19, H 7.36, N 5.51%. μ_{eff} = 3.02 μ_B (300 K).

Method 2. The synthesis of compounds **1** and **2** was carried out in toluene according to *method 1* using [$V^{III}(acac)_3$] in place of [$VOI^{V(}acac)_2$]. Recrystallization from toluene and acetonitrile gave bright–orange crystals of **1** and **2** · 0.25CH_3CN, respectively. The analysis and crystal date proved them to be identical to those obtained by method 1.

1: Yield: 70.0%. Calcd for $C_{25}H_{33}N_2O_4V$: C 63.00, H 6.98, N 5.88. Found: C 62.94, H 6.96, N 5.84%. Unit cell parameters: a = 12.011(3) Å, b = 14.728(3) Å, c = 13.307(3) Å, β = 97.28(2)°.

2·0.25CH_3CN: Yields: 91.5%. Calcd for $C_{27}H_{37}N_2O_4V$·0.25CH_3CN ($C_{27.5}H_{37.75}N_{2.25}O_4V$): C 64.26, H 7.40, N 5.55. Found: C 64.25, H 7.41, N 5.56%. Unit cell parameters: a = 13.237(3) Å, b = 15.650(4) Å, c = 25.711(7) Å, β = 99.83(3)°.

[($V^{IV}O$)$_2$(μ–$L^{1–3}$–κ^4O,N,N,O)$_2$] (L^1, 3; L^2, 4; L^3, 5) and [$V^{IV}O$(μ–$L^{4,5}$–κ^4O,N,N,O)] (L^4, 6; L^5, 7). ***Method A***. A mixture of [$VO(acac)_2$] and $H_2L^{1–5}$ (1 : 1 ratio) in acetonitrile or ethanol (50 cm^3) was refluxed, whereupon the solution turned from blue–green to dark violet over the course of at least 24 h. Then the post–reaction mixture was left for slow cooling to room temperature. After few days, bright–violet crystals of **3**, **4**·2CH_3CN, **5**·2CH_3CN and **6** suitable for X–ray studies were formed. Compound **7** precipitated as a dark violet solid in hot acetonitrile. The products were filtered off, washed with cold CH_3CN, and dried in *vacuo*. In case of reactions in ethanol, the resulting in a dark violet solids were washed with hot acetonitrile to give bright violet microcrystalline products. Compounds **3**–**7** were characterized as follows:

3: Yield: 48.5%. Calcd for $C_{68}H_{108}N_4O_6V_2$: C 69.24, H 9.23, N 4.75. Found: C 69.12, H 9.18, N 4.68%. IR (mineral oil mulls, cm^{-1}): ν(V=O), 960 (s, shr). μ_{eff} = 3.05 μ_B (300 K).

4·2CH_3CN: Yield: 51.0%. Calcd for $C_{44}H_{58}N_6O_6V_2$: C 60.82, H 6.73, N 9.61. Found: C 60.94, H 6.60, N 9.62%. IR (mineral oil mulls, cm^{-1}): ν(V=O), 947 (s, shr). μ_{eff} = 2.96 μ_B (300 K).

5·2CH_3CN: Yield: 49.0%. Calcd for $C_{40}H_{46}Cl_4N_6O_6V_2$: C 50.54, H 4.88, N 8.84. Found: C 50.18, H 4.83, N 8.89%. IR (mineral oil mulls, cm^{-1}): ν(V=O), 959 (s, shr). μ_{eff} = 2.30 μ_B (290 K).

6: Yield: 53.0%. Calcd for $C_{22}H_{30}N_2O_3V$: C 62.70, H 7.18, N 6.65. Found: C 62.63, H 7.17, N 6.58%. IR (mineral oil mulls, cm^{-1}): ν (V=O), 963 (s). μ_{eff} = 1.99 μ_B (300 K).

7: Yield: 69.3%. Calcd for $C_{18}H_{18}Br_4N_2O_3V$: 31.75, H 2.66, N 4.11. Found: C 31.74, H 2.71, N 4.12%. IR (mineral oil mulls, cm^{-1}): ν(V=O), 987 (s). μ_{eff} = 1.84 μ_B (300 K).

[$V^{IV}O$(μ–$L^{4,5}$–κ^4O,N,N,O)] (L^4, 6; L^5, 7). ***Method B***. Compound **6** and **7** were synthesized by applying slight modifications of a procedure described previously by us for **3**–**5**.[Error! Bookmark not defined.a] To *in situ* generated [$V^{V}O$(L–κ^4O,N,N,O)(OPr)] (equimolar amounts of [$VO(OPr)_3$] and H_2L=$H_2L^{4,5}$ in CH_3CN stirred for 2 h) NH_2NMe_2 (1 equiv. for V) was added. The mixture was stirred for 24 hours at room temperature yielding dark–violet solids of **6** and **7**. They were filtered off, washed with CH_3CN and dried under vacuum.

6: Yield: 85.7%. Calcd for $C_{22}H_{30}N_2O_3V$: C 62.70, H 7.18, N 6.65. Found: C 62.72, H 7.19, N 6.64%. IR (mineral oil mulls, cm^{-1}): ν (V=O) 964 (s). Diluted bright-violet filtrate left at room temperature for few weeks produced few dark-violet crystals confirmed by X-ray analysis to be identical to **6** obtained by method 1.

7: Yield: 98.0%. Calcd for $C_{18}H_{18}Br_4N_2O_3V$: 31,75, H 2.66, 4.11. Found: C 31.85, H 2.68, N 4.10%. IR (mineral oil mulls, cm^{-1}): ν (V=O), 988 (s).

Reactions of 4 and 6 with $H_2L^{2,4}$ and Hacac. **(a)** Compounds **4** and **6** (0.5 mmol), Hacac (1.0 mmol), and $H_2L^{2,4}$ (1.0 mmol) in toluene or n-hexane (10 cm^3) were heated under reflux for 24 h. The resulting brown solutions were evaporated to dryness, and the residues recrystallized from toluene or CH_3CN, and identified as **1** and **2**, respectively by elemental analysis and unit cell parameters.

1: Yields: 49.5%. Calcd for $C_{25}H_{33}N_2O_4V$: C 63.00, H 6.98, N 5.88. Found: C 63.09, H 7.01, N 5.89%. Unit cell parameters: a = 12.011(3) Å, b = 14.728(3) Å, c = 13.307(3) Å, β = 97.28(2)°.

2·0.25CH_3CN: Yields: 40.0%. Calcd for $C_{27}H_{37}N_2O_4V$·0.25CH_3CN ($C_{27.5}H_{37.75}N_{2.25}O_4V$): C 64.26, H 7.40, N 5.55. Found: C 64.31, H 7.53, N 5.51%. Unit cell parameters: a = 13.237(3) Å, b = 15.650(4) Å, c = 25.711(7) Å, β = 99.83(3)°.

(b) The reactions of **4** or **6** with Hacac and $H_2L^{2,4}$ were carried out according to procedure **(a)** using acetonitrile or ethanol. Neither color change nor the formation of new products were observed after refluxing the reaction mixture for two days.

General instrumentation

Infrared spectra were recorded on a Perkin–Elmer 180 spectrophotometer in Nujol mulls. Microanalyses were conducted on a Vario EL III CHNS Elemental Analyzer (in–house).

The X–band electron paramagnetic resonance (EPR) spectra of the oxidovanadium(IV) complexes were measured using a Bruker ELEXYS E 500 Spectrometer equipped with NMR teslametr and X–band frequency counter. High–frequency EPR spectra were recorded on the 17 T transmission instrument of the EMR facility. The instrument is equipped with a

superconducting magnet (Oxford Instruments) capable of reaching a field of 17 T. Microwave frequencies over the range 52–630 GHz were generated by a phase–locked Virginia Diodes source, producing a base frequency of 8–20 GHz, which was multiplied by a cascade of frequency multipliers. The instrument is a transmission–type device and uses no resonance cavity.[38] Both the X–Band and high–field EPR spectra were simulated using computer programs written by one of us.[39]

The magnetic susceptibility measurements were made on a Quantum Design MPMS–3 SQUID magnetometer in the temperature range 1.8−300 K in magnetic field of 0.5 T. The susceptibilities of **1**–**6** have been corrected for the diamagnetic contribution by using the Pascal's constants.[40]

X–ray diffraction data for **1**, **4** and **5** were collected on an Xcalibur PX diffractometer with CCD Ruby camera and for **2**, **3** and **6** on a KM4 diffractometer with a CCD graphite camera and Mo Kα radiation (λ = 0.71073 Å) at 100 K.[40] The experimental details and crystal data are given in Table S1 in Supporting Information. The structures were solved by direct methods and refined by the full–matrix least–squares techniques on all F2 data, using the SHELXTL software.[41] All non–hydrogen atoms were refined with anisotropic thermal parameters. All hydrogen atoms were placed in geometrically calculated positions and refined using a riding model with U_{iso} set at $1.2U_{eq}$(C) for aromatic and methylene H atoms, and $1.5U_{eq}$(C) for methyl H atoms. In **3**, the C atoms of methyl groups in the $C(CH_3)_2CH_2C(CH_3)_3$ substituent are disordered and they were modeled and refined in two positions with site occupancy factors (s.o.f.) equal 0.907 and 0.093.

CCDC reference numbers: 1997038 for **1**, 1997039 for **2**·0.25CH_3CN, 1997040 for **3**, 1997041 for **4**·2CH_3CN, 1997042 for **5**·2CH_3CN and 1997043 for **6**·2CH_3CN.

Conflicts of interest

There are no conflicts to declare.

Acknowledgements

The authors thank the National Scientific Centre (Narodowe Centrum Nauki) for financial support of this work. (Poland, grant No: 2012/05/N/ST5/00697). The National High Magnetic Field Laboratory is supported by the National Science Foundation through the Cooperative Agreement DMR–1644779 and the State of Florida.

Notes and references

‡ **ASSOCIATED CONTENT**

† Electronic supplementary information (ESI) available:
Additional crystallographic data for **1**, **2**, **3**–**6**; X-band and HF EPR spectra for **3**–**7** and for **2**, respectively; additional magnetic data for **3**–**5** (PDF), XRD data for **1**, **2** and **3**–**7** (CIF).

1 (a) D. C. Crans, J. J. Smee, E. Gaidamauskas,; L. Yang, *Chem. Rev*., 2004, **104**, 849–902, (b) B. A. MacKay, M. D. Fryzuk, *Chem. Rev*., 2004, **104**, 385–402, (c) D. Rehder, *Bioinorganic Vanadium Chemistry*, John Wiley & Sons, Ltd.: New York, 2008.

2 (a) O. Kahn, *Molecular Magnetism*, VCH, NewYork, 1993. (b) D. Christou, D.Gatteschi, D. N. Hendrickson, R. Sessoli, *MRS Bull.*, 2000, **25**, 66–71. (c) W. Plass, *Angew. Chem. Int. Ed. Engl*., 1996, **35**, 627–631, (d) M. Tsuchimoto, N. Yoshioka, *Chem. Phys. Lett*., 1998, **297**, 115–120, (e) W. Plass, Z. Anorg. Allg. Chem. 1997, 623, 1290-1298.

3 (a) E.Tsuchida, K. Oyaizu, *Coord. Chem. Rev*., 2003, **237**, 213–228. (b) J. C. Pessoa, I. Correia, *Coord. Chem. Rev*., 2019, **388**, 227–247, (c) Y. Chen, S. Yekta, , A. K. Yudin, *Chem. Rev*., 2003, **103**, 3155–3211, (d) M. Debnath, A. Dutta, S. Biswas, K. K. Das, H. M. Lee, J. Vicha, R. Marek, J. Marek, M. Ali, *Polyhedron,* 2013, **63**, 189-198.

4 (a) M. R. Maurya, A. A. Khan, A. Azam, S. Ranjan, N. Mondal, A. Kumar, F. Avecilla, J. C. Pessona, *Dalton Trans*., 2010, **39**, 1345–1360, (b) L. Reytman, O. Braitbard, E. Y. Tshuva, *Dalton Trans*., 2012, **41**, 5241–5247, (c) O. Taheri, M. Behzad, A. Ghaffari, M. Kubicki. G. Dutkiewicz, A. Bezaatpour, H. Nazari, A. Khaleghian, A. Mohammadi, M. Salehi, *Trans. Met. Chem.* 2014, **39**, 253–259.

5 (a) E. Kober, Z. Janas, J. Jezierska, *Inorg. Chem*., 2016, **55**, 10888–10898, (b) P. Adão, J. C. Pessoa, R. T. Henriques, M. L. Kuznetsov, F. Avecilla, M. R. Maurya, U. Kumar, I. Correia, *Inorg. Chem*., 2009, **48**, 3542-3561, (c) P. Adão, M. R. Maurya, U. Kumar, F. Avecilla, R. T. Henriques, M. L. Kuznetsov, J. C. Pessoa, I. Correia, *Pure Appl. Chem*., 2009, **81**, 1279-1296, (d) I. Correia, J. C. Pessoa, M. T. Duarte, M. F. Minas da Piedade, T. Jakusch, T. Kiss, A. Dörnyei, M. M. C. A. Castro, C. F. G. C. Geraldes, F. Avecilla, *Eur. J. Inorg. Chem.,* 2005, 732-744, (e) I. Correia, J. C. Pessoa, M. T. Duarte, R. T. Henriques, M. F. Minas da Piedade, L. F. Veiros, Jakusch, T. Kiss, A. Dörnyei, M. M. C. A. Castro, C. F. G. C. Geraldes, F. Avecilla, *Eur. J. Inorg. Chem*., 2004, 2301-2317, (f) P. Adão, J. C. Pessoa, R. T. Henriques, M. L. Kuznetsov, F. Avecilla, M. R. Maurya, U. Kumar, I. Correia, *Inorg. Chem*., 2009, **48**, 3542–3561.

6 M. M. Hänninen, A. Peuronen, P. Damlin, V. Tyystjärvi, H. Kivelä, A. Lehtonen, *Dalton Trans*., 2014, **43**, 14022–14028.

7 (a) T. K. Paine, T. Weyhermüller, L. D. Slep, F. Neese, E. Bill, E. Bothe, K. Wieghardt, P. Chaudhuri, *Inorg. Chem*., 2004, **43**, 7324–7338, (b) A. Jezierski, J. B. Raynor, J. Chem. Soc., Dalton Trans., 1981, 1.

8 T. Kajiwara, R. Wagner, E. Bill, T. Weyhermüller, P. Chaunhuri., *Dalton Trans*., 2011, **40**, 12719–12726.

9 S. R. Cooper, Y. B. Koh, K. N. Raymond, *J. Am. Chem. Soc*. 1982, **104**, 5092–5102.

10 P. R. Klich, A. T. Daniher, P. R. Challen, D. B. McConville, W. J. Youngs, *Inorg. Chem*., 1996, **35**, 347-356.

11 (a) Z. Liu, F. C. Anson, *Inorg. Chem*., 2000, **39**, 274–280, (b) Z. Liu, F.C. Anson, *Inorg. Chem*. 2001, **40**, 1329–1333, (c) E. Raamat , K. Kaupmees, G. Ovsjannikov, A. Trummal , A. Kütt, J. Saame, I. Koppel, I. Kaljurand, L. Lipping, T. Rodima, V. Pihl, I. A. Koppel, I. Leito, *J. Phys. Org. Chem*. 2013, **26.** 162–170, (d) AG. Cook, PM Feltman, *J. Chem. Educ*. 2007, **84**, 1827–1829.

12 (a) T. Sakumaroto, T. Moriuchi, K. Hirao, *J. Inorg. Biochem*. 2016, **164**, 77–81, (b) T. Moriuchi, K. Ikeuchi, K. Hirao, *Dalton Trans.,* 2013, 11824–11830, (c) Z. Janas, P. Sobota, *Coord. Chem. Rev.*, 2005, **249,** 2144–2155, (d) R. A. Henderson, Z. Janas, L. B. Jerzykiewicz, R. L. Richards, P. Sobota, *Inorg. Chim. Acta* 1999, **285**, 178–183, (e) S. C. Davies, D. L. Hughes, Z. Janas, L. Jerzykiewicz, R. L. Richards, J. R. Sanders, P. Sobota, *Chem. Commun*., 1997, 1261–1262, (f) C. Le Floc'h, R. A. Henderson, P. B. Hitchcock, D. L. Hughes, Z. Janas, R. L. Richards, P. Sobota, S. Szafert, *J. Chem. Soc*. *Dalton Trans*. 1996, 2755–2762.

13 T. A. Immel, U. Groth, T. Huhn, *Chem. Eur. J.*, 2010, **16**, 2775–2789,

14 (a) P. Subramanian, J. T. Spence, R. Ortega, J. H. Enemark, *Inorg. Chem.*, 1984, **23**, 2564–2572, (b) C. J. G. Hinshaw, J. T. Peng, J. H. Spence, M. Enemark, L. Bruck, J. Kristofzski, S. L. Merbs, R. Ortega, P. A. Wexler, *Inorg. Chem.* 1989, **28**, 4483–4491, (c) Y.–L Wong, J.–F Ma, W.–F Law, Y. W.–T. Wong, Z.–Y Zhang, T. C. W Mak, D. K. P. Ng, *Eur. J. Inorg. Chem.* 1999, 313–321, (d) E. Y. Tshuva, I. Goldberg, M. Kol, *J. Am. Chem. Soc.,* 2000, 10706–10707, (e) J. Balsells, P. J. Carroll, P. J. Walsh, *Inorg. Chem*., 2001, **40**, 5568–5574, (f) S. Segal, I. Goldberg, M. Kol, *Organometallics*, 2005, **24,** 200–202, (g) J. England, C. R. Davies, M. Banaru, A. J. P. White, *Adv. Synth. Catal*. 2008, **350**, 883–897, (h) T. A. Immel, U. Groth, T. Huhn, *Chem. Eur. J.,* 2010, **16**, 2775–2789, (i) D. Peri, S. Meker, C. M. Manna, E. Y. Tshuva, *Inorg. Chem.,* 2011, **50,** 1030–1038, (j) T. Karimpur, E. Safaei, A. Wojtczak, Z. Jagličič, A. Kozakiewicz, *Inorg. Chim. Acta*, 2013, **395**, 124–134.

15 (a) C. Lorber, F. Wolff, R. Choukroun, L. Vendier, *Eur. J. Inorg. Chem.,* 2005, 2850–2859; (b) S. Groysman, S. Segal, M. Shamis, I. Goldberg, M. Kol, Z. Goldschmidt, E. Hayut-Salant, J. Chem. Soc., Dalton Trans., 2002, 3425–3426. (c) A.W. Addison, T.N. Rao; J. Reedijk; J. Rijn; G.C. Verschoor, *J. Chem. Soc. Dalton Trans*. 1984, 1349–1356.

16 (a) G. Hoshina, M. Tsuchimoto, S. Ohba, *Acta, Cryst*. 1999, **C55**, 1812–1813, (b) G. Hoshina, M. Tsuchimoto, S. Ohba, K. Nakajima, H. Uekusa, Y. Ohashi,; H. Ishida, M. Kojima, *Inorg. Chem.*, 1998, **37**, 142–145, (c) C. R. Cornman, K. M. Geiser–Bush, S. P. Rowley, P. D. Boyle, *Inorg. Chem*., 1997, **36**, 6401–6408.

17 (a) J. Krzystek, A. Ozarowski, J. Telser, D. C. Crans, *Coord. Chem. Rev.*, 2015, **301–302**, 123–133. (b) S. Ye, F. Neese, A. Ozarowski,; D. Smirnov, J. Krzystek, J. Telser, J.–H. Liao, Ch.–H. Hung, W.Ch. Chu,. Y.–F. Tsai, Ch. Wang. R.–Ch Chen, H.–F. Hsu, *Inorg. Chem,.* 2010, **49**, 977–988.

18 A. Ozarowski, D. Reinen, *Inorg. Chem*., 1986, **25**, 1704–1708.

19 B. Bleaney, K. D. Bowers, Proc. Roy. Soc. London Ser. A, 1952, 214, 451–465.

20 R. Maurice, K. Sivalingam, D. Ganyushin, N. Guihery, C. de Graaf, F. Neese, *Inorg. Chem.*, 2011, **50**, 6229–6236.

21 A. Ozarowski, C.J. Calzado, R.P. Sharma, S. Kumar, J. Jezierska, C. Angeli,; F. Spizzo, V. Ferretti, *Inorg. Chem.*, 2015, **54**, 11916–11934.

22 J. Bendix, M. Brorson C. E. Schaeffer, *Inorg. Chem*., 1993, **32**, 2838–2849.

23 N. D. Chasteen, Biological Magnetic Resonance, Vol. 3 (Eds.: L. J. Berliner, J. Reuben), Plenum, New York, 1981. p. 53–119. Fig. 17.

24 (a) A. S. Ceccato, A. Neves, M. A. de Brito, S. M. Drechsel, A. S. Mangrich, R. Werner, W. Haase, A. J. Bortoluzzi, *J. Chem. Soc., Dalton Trans.*, 2000, 1573–1577., (b) M. Mikuriya, M.Fukuya, *Bull. Chem. Soc. Jpn.,* 1996, **69**, 679–683. (c) A. Neves, K. Wieghardt, B. Nuber, J. Weiss, *Inorg. Chim. Acta*, 1988, **150**, 183–187., (d) K. Wieghardt, U. Bossek, K. Volckmar, W. Swiridoff, J. Weiss, *Inorg. Chem.*, 1984, **23**,1387–1389

25 N. F Chilton, R. P. Anderson, L. D. Turner, A. Soncini, K. S. Murray, *J. Comput. Chem.*, 2013, **34**, 1164–1175 Noodleman, L. Valence Bond Description of Antiferromagnetic Coupling in Transition Metal Dimers. J. Chem. Phys. 1981, 74 (10), 5737–5743.

26 L. Noodleman, E. R. Davidson, *Chem. Phys*., 1986, **109** (1), 131–143.

27 J. P. Malrieu, R. Caballol, C. J. Calzado, C. de Graaf, N. Guihéry, *Chem. Rev.*, 2014, **114**, 429–492.

28 A. Rodríguez–Fortea, P. Alemany, S. Alvarez, E. Ruiz, *Inorg. Chem.*, 2002, **41**, 3769–3778.

29 A. Bencini, D. Gatteschi, *J. Am. Chem. Soc*., 1980, **108**, 5763–5771.

30 F. Neese, ORCA – An Ab Initio, Density Functional and Semiempirical Program Package, Version 4.0.1; Surf Sara: Amsterdam 2017. Neese, F. The ORCA Program System. Wiley Interdiscip. Rev. Comput. Mol. Sci. 2012, **2**, 73–78.

31 A. Schäfer, H. Horn, R. Ahlrichs, *J. Chem. Phys*., 1992, **97** (4), 2571–2577.

32 The Ahlrichs auxiliary basis sets (https://www.basissetexchange.org/) have been hardwired into the ORCA software.

33 K. Eichkorn, F. Weigend, O. Treutler, R. Ahlrichs, *Theor. Chem. Accounts Theory, Comput. Model.* (Theoretica Chim. Acta) 1997, **97** (1–4), 119–124.

34 C. Duboc, D. Ganyushin, K. Sivalingam, M.–N. Collomb, F. Neese, *J. Phys. Chem. A,* 2010, **114**, 10750–10758.

35 A. Pascual–Alvarez, J. Vallejo, E. Pardo, M. Julve, F. Lloret, J. Krzystek, D. Armentano, W. Wernsdorfer, J. Cano, *Chem. Eur. J.,* 2015, **21**, 17299–17307.

36 F. Weigend, R. Ahlrichs, *Phys. Chem. Chem. Phys*., 2005, **18**, 3297-3305.

37 C. J. Whiteoak, G. J. P. Britovsek,. V. C. Gibson, A. J. White, *Dalton Trans.*, 2009, 2337–2344.

38 A. Hassan, L. Pardi, J. Krzystek, A. Sienkiewicz, P. Goy, M. Rohrer, L.–C. Brunel, *J. Magn. Reson*., 2000, **142** (2), 300–312.

39 G. A. Bain, J. F. Berry, *J. Chem. Ed.*, 2008, **85**, 532–536.

40 CrysAlis CCD and CrysAlis RED, Oxford Diffraction: Wrocław, Poland, 2009.

41 G. Sheldrick, *Acta Cryst. C* 2015, **71**, 3-8.